Scientific Research Publishing

Journal of Minerals and Materials Characterization and Engineering, 2025, 13(3), 63-82
https://www.scirp.org/journal/jmmce
ISSN Online: 2327-4085
ISSN Print: 2327-4077

Erosive-Corrosive Wear of Thermally Sprayed Hard Coatings Using Powder and Wire Materials

Roberto Sagaró Zamora[1], Hipólito Carvajal Fals[2], Mario Sanchez Orozco[1], Carlos Roberto Camello Lima[3]*

[1]Faculty of Mechanical Engineering, University of Oriente, Santiago de Cuba, Cuba
[2]Faculty of Mechanical Engineering, Federal University of Technology of Paraná, Ponta Grossa, Brazil
[3]School of Engineering, Mackenzie Presbyterian University, São Paulo, Brazil
Email: sagaro@uo.edu.cu, mario@uo.edu.cu, hcf151@yahoo.es, *carlos.lima@mackenzie.br

How to cite this paper: Zamora, R.S., Fals, H.C., Orozco, M.S. and Lima, C.R.C. (2025) Erosive-Corrosive Wear of Thermally Sprayed Hard Coatings Using Powder and Wire Materials. *Journal of Minerals and Materials Characterization and Engineering*, **13**, 63-82.
https://doi.org/10.4236/jmmce.2025.133005

Received: April 11, 2025
Accepted: May 27, 2025
Published: May 30, 2025

Abstract

Erosive-corrosive wear experiments were conducted on coatings deposited by flame spray/flexicord and high velocity oxy-fuel (HVOF) thermal spray techniques onto AISI 1020 steel substrates. Erosion tests were performed on the slurry tribometer using a combination of freshwater with quartz sand particles with a grain size of 300 to 425 μm. The study of the erosive-corrosive effect was carried out by comparing the results obtained in electrochemical corrosion tests of original and previously eroded samples, as well as samples subjected to erosive-corrosive tests under the most critical condition. A solution of 0.1 M H_2SO_4, with 19 g/L of Cl was used as the corrosive medium. All the coatings exhibited erosion wear mechanisms associated with brittle forms of failure due to high hardness. The worst erosion test condition was for the impact velocity of the particles of 9.33 m/s at the impact angle of 90˚. Under this condition, the erosion rate was 78.28 mm^3/Kg for the FS/FC sprayed coating and 25.37 mm^3/Kg for the HVOF coating. Under corrosive wear conditions, the process was predominantly influenced by the erosive component, which was favored by the low resistance to corrosion of the binder phase. The degradation mechanisms are related to the dilution of the binder phase at the interface and the extrusion of hard fillers. Factors such as the composition and microstructure of the deposits, porosity, roughness, and corrosion significantly influenced the test results. The wear mechanism reveals that the erosive component prevails in the wear-corrosion synergy.

Keywords

Erosion, Corrosion, Thermal Spray, Flexicord, Hard Coatings

1. Introduction

Often in industrial practice, performance, durability, and reliability are directly or indirectly related to some type of wear, which limits the useful life of 80% of machine components [1] [2]. Recently, as a rational and economic compromise between surface properties and the volume of the material, the science of surface engineering has stimulated the development of coating techniques or surface modifications of the base material, adequate to withstand the increasing stresses that are increasingly required of material surfaces [3] [4]. Thermal spray technology for the deposition of ceramic materials, metal alloy compounds, and super alloys is frequently used as the most suitable approach in the dynamics between wear, maintenance, and cost in machine elements that must operate in conditions of severe wear and in very corrosive environments, such as mining, the paper processing industry, aeronautics, and power generation, among others [5] [6].

The coating behavior under conditions of erosive-corrosive wear depends largely on its composition and microstructure, which are related to the starting material and processing. The evolution of the HVOF technique in recent times has been characterized by the use of novel compositions and nanostructured powders. The flame spraying flexicord technique (FS/FC) is the simplest of thermal spraying techniques, modified by applying novel feedstock materials called flexicords. The powder particles of the feedstock material are bonded in a polymer that allows the uniform distribution of the particles inside the cord wire. It is considered by its producers [7] as an alternative to create dense ceramic coatings of carbides and metal base with low porosity and surface roughness, with less deterioration of the stoichiometry and low internal residual stresses for better impact resistance. Their cost, when compared with the HVOF method, is lower by around 9% [8] [9].

This work presents a comparative analysis of the behavior of several coatings deposited by HVOF and FS/FC under corrosive wear conditions, considering the influence of operational variables such as the angle of impact and the speed of the abrasive particles, as well as the chemical composition and microstructure of the deposits, relating the latter to the method of deposition.

2. Materials and Methods

2.1. Processes and Material Characteristics

The coatings were achieved through two techniques related to thermal spray, specifically the HVOF technique, where the materials used were commercial, agglomerated, and sintered powders, WC10Co4Cr (1350 VM/WC-731-1, Praxair, Concord, NH, USA) −45/+15 µm and Wall Colmonoy® (88HV) +5/+10 µm. Using Flame Spray FlexiCords (FS/FC), the 15HC Hardkarb and RocDur62 (Saint Gobain, Worcester, MA, USA) were deposited, both with a nominal diameter of 4.75 ± 0.1 mm. The chemical composition and density values of the materials are displayed in **Table 1**. The substrate used was AISI 1020 low carbon steel.

Table 1. Density and chemical composition of the feedstock materials.

Materials	Density (g/cm^3)	Chemical composition (% Wt)								
		C	W	Co	Cr	B	Ni	Si	Mo	Fe
1350 VM	10.1	5.40	Bal.	10.1	4.2					
COLMONOY 88HV	10.1	0.80	16.5	-	15.0	3.0	Bal.	4	-	3.50
15HC	13.3	5.40	Bal.	0.4	2.7	-	10.7	-	2.70	1.00
RocDur 62	8.2	0.62	-	-	14.1	2.92	Bal.	3.82	-	3.52

For coatings deposited through the FS/FC method, a Master Jet 2 gun was used and. For the HVOF method, a JP 5000 system (Praxair TAFA) was employed. The main parameters used in both processes are shown in Table 2.

Table 2. Parameters adopted for the thermal spray processes.

HVOF thermal spray process						
Material	Designation	Nozzle (mm)	Standoff Distance (mm)	Oxygen (SLPM)	Nitrogen (SLPM)	Kerosene (GLP)
1350 VM/WC-731-1	HVOF 1350	101.6	350 ÷ 400	873.09	11.799	6.0
Colmonoy 88HV	HVOF 88HV	101.6	350 ÷ 400	920.28	10.855	5.5
FS/FC thermal spray process						
Material	Designation	Compressed Air (Bar)	Standoff Distance (mm)	Oxygen (SLPM)	Acetylene (SLPM)	Feeding (m/s)
HardKarb 15HC	FS/FC 15HC	4.5	100 ÷ 150	50	60	0.0076
RocDur62	FS/FC RocDur62	4 ÷ 5	100 ÷ 150	50	60	0.0075

Figure 1(a) and Figure 1(b) show images of the micrograph of the powder used in the HVOF technique, the enlarged details of the images (upper right corner) exhibit agglomerate and sintered particles of spherical morphology. In Figure 1(c) and Figure 1(d) the images of the scanning electron microscopy show the micrograph of the cross section of the cord wire materials, exhibiting in the enlarged details agglutinated spherical particles.

2.2. Microstructural Characterization and Mechanical Properties

The microstructure of the coatings was characterized by optical microscopy (OM) techniques using a NIKON equipment, model OPTPHOT, and by scanning electron microscopy using a JEOL-JXA 840 equipment. The roughness of the coatings once deposited was obtained by means of a MITUTOYO SUFTEST 211. The microhardness measurements were done in a Vickers indenter (SHIMADZU model HMV-G), with an indentation load of 0.3 Kg and a dwell time under the load of 15 s. The thickness of the coatings was measured for each deposit by optical microscopy with the use of IMAGE-PRO-PLUS software. For the calculation of the fracture toughness of the samples, the load applied was 2 kg for the coatings obtained by the HVOF method and 1 kg for those obtained with FS/FC, the dwell time of the load in both cases was 20 s. The calculation of the fracture toughness of the coatings (kc) was made through the equation of Evans and Wilshaw [10], related to Palmqvist radial cracks.

Porosity analysis was conducted utilizing SEM microscopy and image processing techniques. The software used was ImageJ 1.48 V. The images selected for analysis were magnified to 500X. The pore count was performed in six areas of comparable dimensions corresponding to the cross sections of each coating, allowing for the calculation of an average percentage of pores from the six measurements taken.

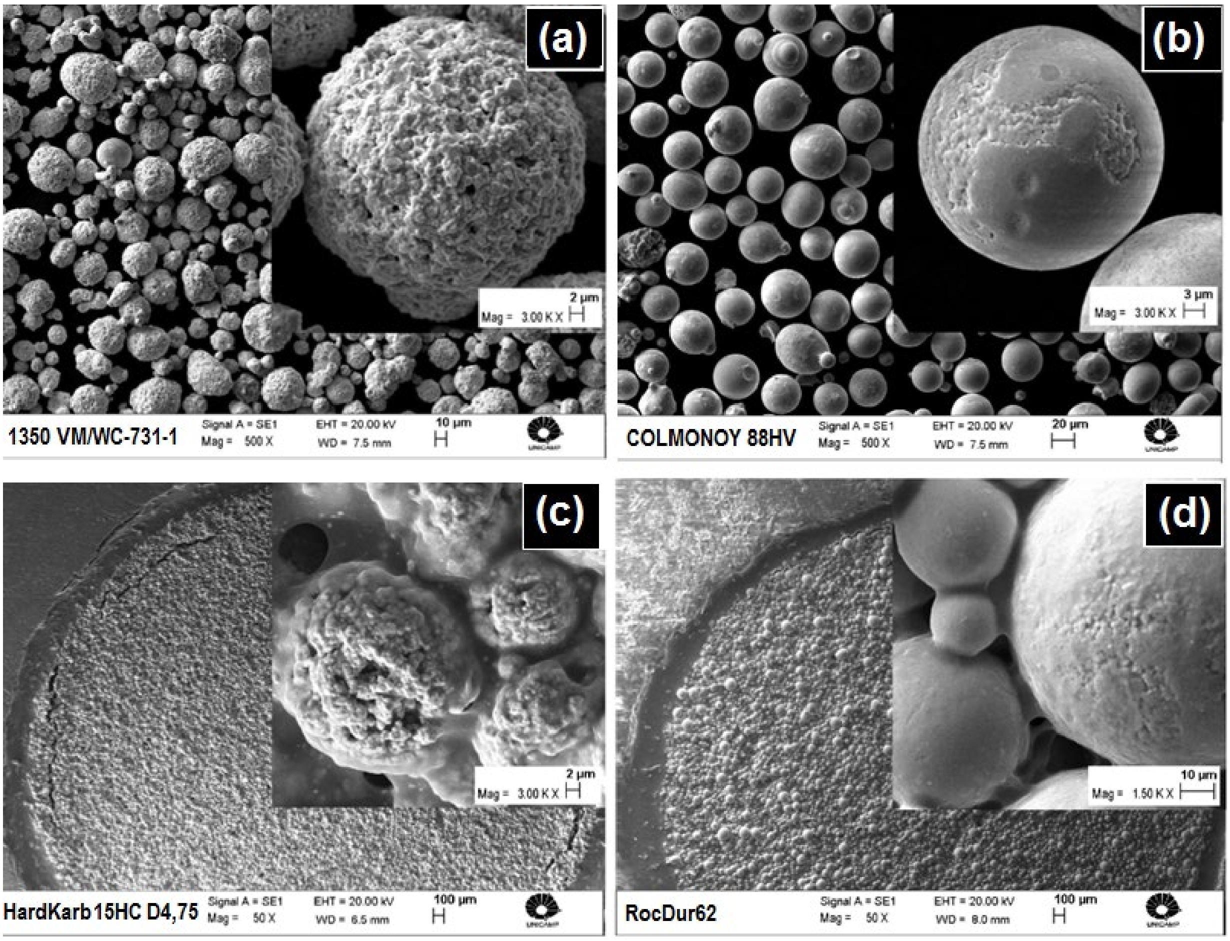

Figure 1. SEM images of the materials: (a) 1350 VM/WC-731-1; (b) Colmonoy 88HV; (c) Hardkarb 15HC D4.75; (d) RocDur62.

2.3. Erosion Tests

The erosion tests were carried out using a pot type slurry erosion tribometer described elsewhere [11] [12]. Samples for the tests were obtained from deposits in the form of prismatic bodies of (10 × 8 × 4) mm. The roughness of the test bodies corresponded to coating conditions. The abrasive mixture used consists of fresh water (700 ml) and a concentration of abrasive particles of 300 g of quartz sand (SiO_2—30/40 SE) with grain size between 300 to 425 μm and HV = 1100 HV.

The design of the sampling device allowed to evaluate an impact angle of the abrasive particles $\alpha = 30^\circ$ and 90°. The circular plates rotate with 660 and 1550 rpm with an instantaneous cylindrical velocity (v) of 3.61 and 9.33 m/s, respectively. The impact velocities and angles of the eroding particles were used due to the limitations of the pot type slurry erosion tribometer configuration used in the erosion tests. However, coatings like WC-Co and other ceramics typically exhibit maximum erosion at normal impact angles (90˚), indicating brittle fracture mechanisms, as confirmed in the work of Kumar *et al.* [13].

The tests were performed for 6 hours at 1-hour intervals, in which the erosion rate was determined. The wear was determined by difference of the weight losses of the samples before and after each run. Each trial was repeated 3 times. Weight losses were measured, and results are reported as the volume of eroded material per unit mass of erodent particles used during the tests. The results of mass losses were obtained by weight difference determined sample volume loss (Ww) with the following expression:

$$W_v = \frac{Ww \times 1000}{\rho} \tag{1}$$

$$Er = \frac{Wv}{m} \tag{2}$$

where: Wv is the loss of volume (mm^3), Ww the loss of mass (g) and ρ the material density as deposit (g/cm^3), Er erosion rate and m was the mass of particles contained in the mixture.

2.4. Erosive-Corrosive Wear Tests

For the evaluation of erosive-corrosive wear resistance, polarization curves were determined in samples of original and eroded surfaces, and finally under synergies conditions with v = 9.33 m/s, 6 hours and for impact angle $\alpha = 90^\circ$ (as the most critical conditions). The tests were carried out using a 3-electrode electrochemical cell, where the samples were used as working electrodes, the counter electrode used was platinum (Pt) and the potentials were monitored through an Ag/AgCl electrode in saturated KCl. Once the open circuit potential of the samples (corrosion potential) were determined, the potential varied from a value of −300 mV to 1700 mV. As corrosive agent, 0.1 M H_2SO_4 was used with 19 g/L of CL^-. In each of the cases, microstructural observations were done by SEM after test. For the realization of the tests, the solution was aerated by bubbling for 20 minutes with N_2.

3. Results and Discussion

3.1. Microstructural Characterization and Mechanical Properties

The average thickness of the coatings was 500 µm. The OM images (**Figure 2**) allowed observation of characteristic defects of coatings obtained using the thermal spray technique, such as pores (globular and interlaminar), cracks between the phases, and unmelted particles.

Figure 3 shows the SEM micrograph related to one of the tungsten carbide coatings, deposited through the HVOF and FS/FC methods.

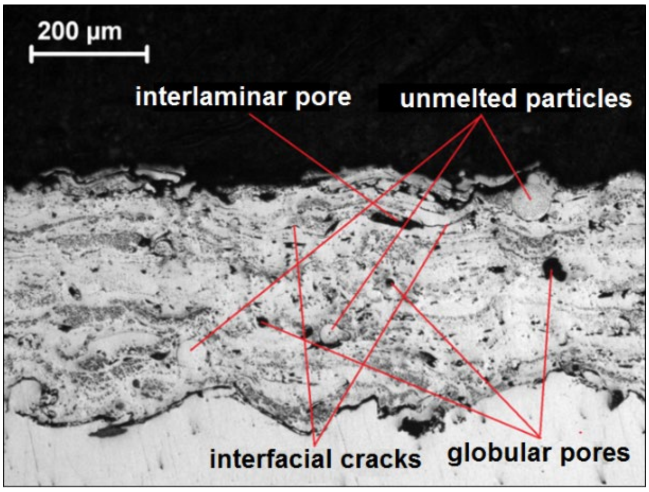

Figure 2. OM image of the cross-section of the composite coating RocDur62 deposited by FS/FC.

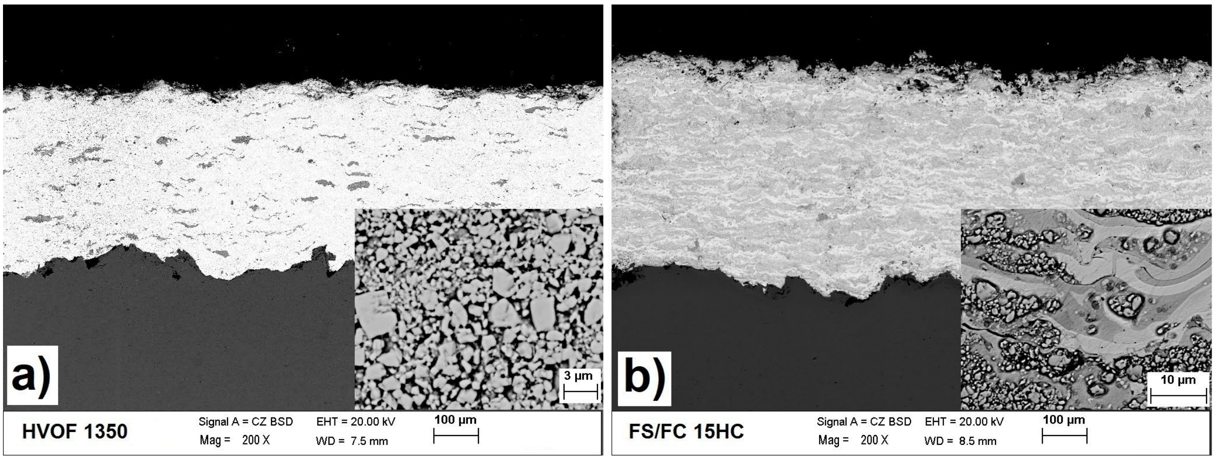

Figure 3. SEM images of the cross-section of the tungsten carbide coating (a) deposited by HVOF (1350) and (b) deposited by FS/FC (15HC).

The SEM micrograph shown in Figure 3(a) presents the microstructure of material 1350, consisting of a dark phase related to the matrix (chrome cobalt) and a clear phase composed of uniformly distributed reinforcing particles (WC). In Figure 3(b), however, the presence of a CrNi matrix with dissolved phases and a more macroscopically heterogeneous distribution of the reinforcing particles can also be observed.

In metallic matrix composite coatings, very fine hard particles, typically carbides and borides precipitated in a Ni base matrix, are observed in the images of Figure 4(a) and Figure 4(b). These particles aim to increase the hardness of the coatings. However, there is a noticeable difference in the microstructures shown, related to the reinforcing particles that can be observed in the SEM image detailed in **Figure 4(b)**, corresponding to the RocDur 62 coating. It shows a more heterogeneous microstructure, less dense, with a less uniform distribution of reinforcement particles. Another important factor is the greater decomposition of the carbide particles that occur during the deposition process due to the low projection velocity of the FS/FC method, making it more prone to decarburization. With the loss of carbon, there is an increase in the binder mean free path (λ) [14]-[16].

As seen in **Figures 2-4**, the coatings deposited by FS/FC exhibited high roughness, a less dense and more porous surface, and some semi-molten particles, along with a less uniform distribution of carbides and cracks (transverse and parallel to the surface) in their topography. All these defects, resulting from the deposition method, are stress incubators, decrease erosion resistance, and negatively affect corrosion resistance [17]-[20].

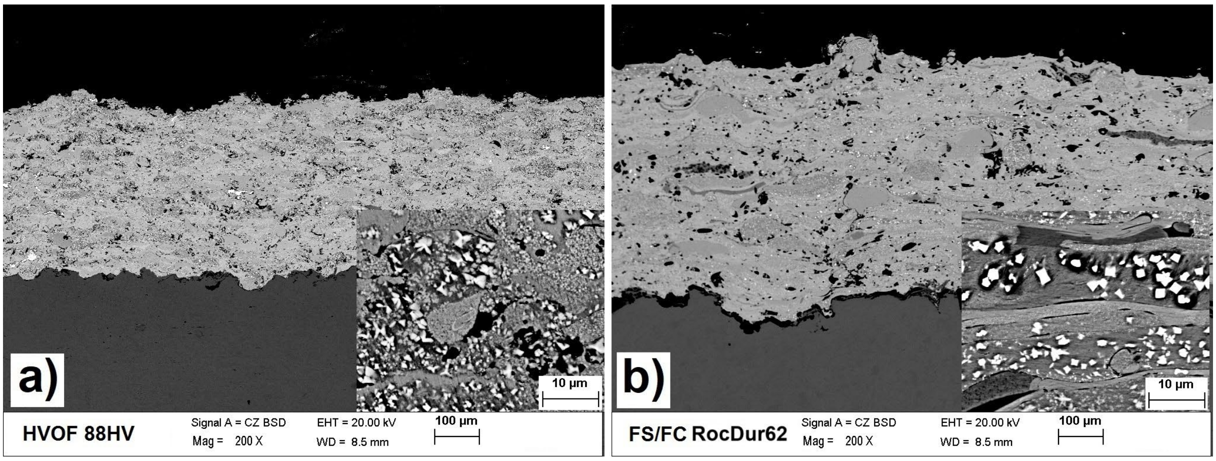

Figure 4. SEM images of the cross-section of metallic matrix coatings (a) HVOF 88HV and (b) FS/FC RocDur62.

The measurements of surface roughness and porosity corroborate the previous statements. **Table 3** shows the results of both parameter measurements for each coating.

Table 3. Results of the surface roughness and porosity measurements for tested materials.

Material	Surface Roughness *Ra* (µm)	Porosity (%)
HVOF 1350	4.42 ± 0.32	0.39 ± 0.04
FS/FC 15HC	8.84 ± 0.20	0.39 ± 0.19
HVOF 88HV	5.97 ± 0.23	4.29 ± 1.17
FS/FC RocDur62	13.07 ± 0.38	5.81 ± 2.94

Table 4 presents a summary of mechanical properties for all materials. As can be seen, the high hardness of the deposits is related to the presence of tungsten and chromium carbides. Also, the presence of boron, even in small quantities causes an increase in the hardness of the alloys. From the table it is observed that the coatings deposited through the HVOF method have higher values of Kc.

Table 4. Mechanical properties of the studied coatings.

HVOF Coatings	Microhardness, *Hv* (GPa)	Fracture toughness, Kc (MPa $m^{1/2}$)	FS/FC Coatings	Microhardness, *Hv* (GPa)	Fracture toughness, *Kc* (MPa $m^{1/2}$)
HVOF 1350	12.01 ± 70.71	9.70 ± 0.15	FS/FC 15HC	7.37 ± 60.26	4.36 ± 0.17
HVOF 88HV	7.43 ± 21.50	6.70 ± 0.43	FS/FC RocDur62	7.19 ± 76.52	3.86 ± 0.22

3.2. Erosion Tests

Considering four experimental conditions related to the speed and impact angle of the erosive particles, the results obtained were statistically processed to identify the differences and similarities in the erosion rate of the coatings, as well as to define the most critical experimental condition. Table 5 shows the average values of the cumulative erosion rate according to the experimental conditions, the type of coating and the deposition methods used.

Table 5. Erosion rate of the coatings.

Material	Erosion rate, Er (mm^3/Kg)			
	$\alpha = 30^\circ$/V = 3.61 m/s	$\alpha = 90^\circ$/V = 3.61 m/s	$\alpha = 30^\circ$/V = 9.33 m/s	$\alpha = 90^\circ$/V = 9.33 m/s
HVOF 1350	2.88 ± 0.75	2.12 ± 0.33	8.39 ± 0.88	9.35 ± 2.14
HVOF 88HV	2.29 ± 0.31	2.19 ± 0.48	15.25 ± 1.97	25.37 ± 6.59
FS/FC 15HC	6.18 ± 1.15	6.37 ± 1.12	36.51 ± 1.84	58.23 ± 12.94
FS/FC RocDur62	4.11 ± 0.15	3.47 ± 0.15	33.46 ± 3.72	78.28 ± 2.79

The statistical analysis of variance (Figure 5) showed that in those experimental conditions where the value of the impact velocity v = 3.61 m/s, regardless of the value of the impact angle, there is similarity in erosion rate between both deposition methods. With the analysis carried out, it can be stated that in these cases it is possible to replace the HVOF deposition method with the FS/FC method to obtain the coatings and thus reduce the cost of the process by 9% [8] [21].

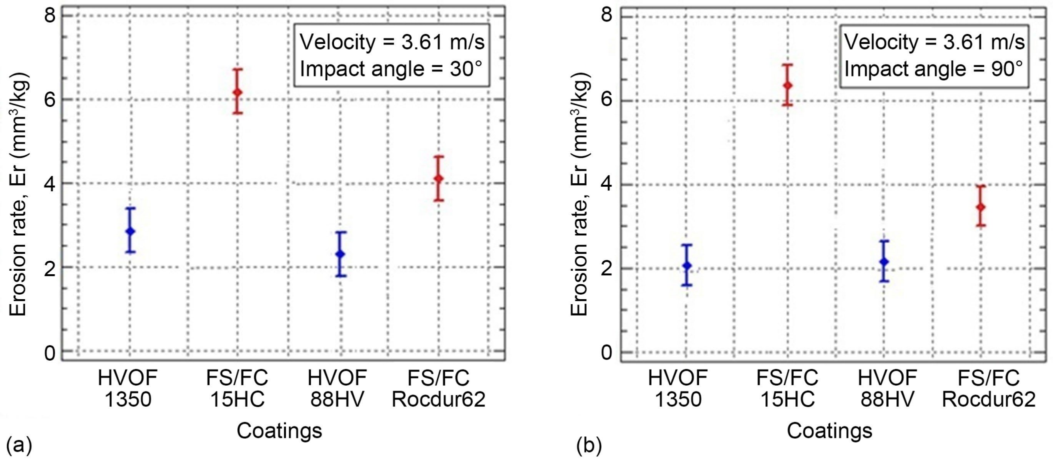

Figure 5. Analysis of variance for the coatings erosion rates. (a) Impact velocity of 3.61 m/s and impact angle of 30˚. (b) Impact velocity of 3.61 m/s and impact angle of 90˚.

The results shown in Table 5 and Figure 6 allow us to deduce that for the coatings deposited with the HVOF method as well as with FS/FC, the highest values of the erosion ratio correspond to the experimental conditions where the impact velocity of the particles is of 9.33 m/s, being the most critical when the impact angle of the particles is 90˚. The coatings deposited by HVOF, presented more homogeneous and dense microstructures, with a more uniform distribution of the reinforcing particles, contributing to a greater resistance to the propagation of cracks that are the cause of the loss of binder matrix adhesion with the reinforcement carbides and its grains extrusion.

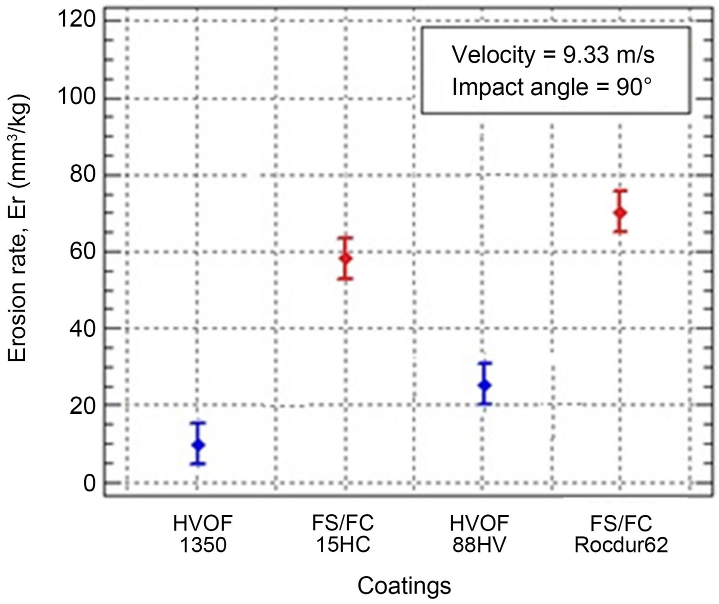

Figure 6. Analysis of variance for erosion rate under the critical condition.

The behavior of the erosion rate in the FS/FC coatings becomes a complex process, due to the not evenly distributed reinforcement carbides and decarburization processes, resulting in undesirable brittle phases that contribute to the propagation of the cracks and the mechanical properties worsening.

The above can be confirmed through the heterogeneous microstructure of the material FS/FC 15HC (Figure 7), as well as the presence of the phase W_2C as a result from decarburization, a fragile phase, causing an area inside the limits of completely and partially molten carbides where cracks easily propagate [22]-[24]. Large volumes of phases containing a high level of dissolved carbon and other components are also observed. These dissolved phases, together with the decarburization of the carbide particles, increase the magnitude of the binder mean free path and for instance the weakening of the mechanical properties (mainly microhardness and fracture toughness) [13] [14] [25].

Beyond these peculiarities, characteristics of the deposition method and the metallographic structure, which results in a higher wear rate of the FS/FC materials, the erosive wear mechanisms for the materials tested comply with the E90/E30 ratio > 1 [25] [26], indicating its fragile nature. The peculiarities of this mechanism include degradation of the metallic phase, extrusion of the carbide grains and propagation and growth of the cracks (**Figure 8**).

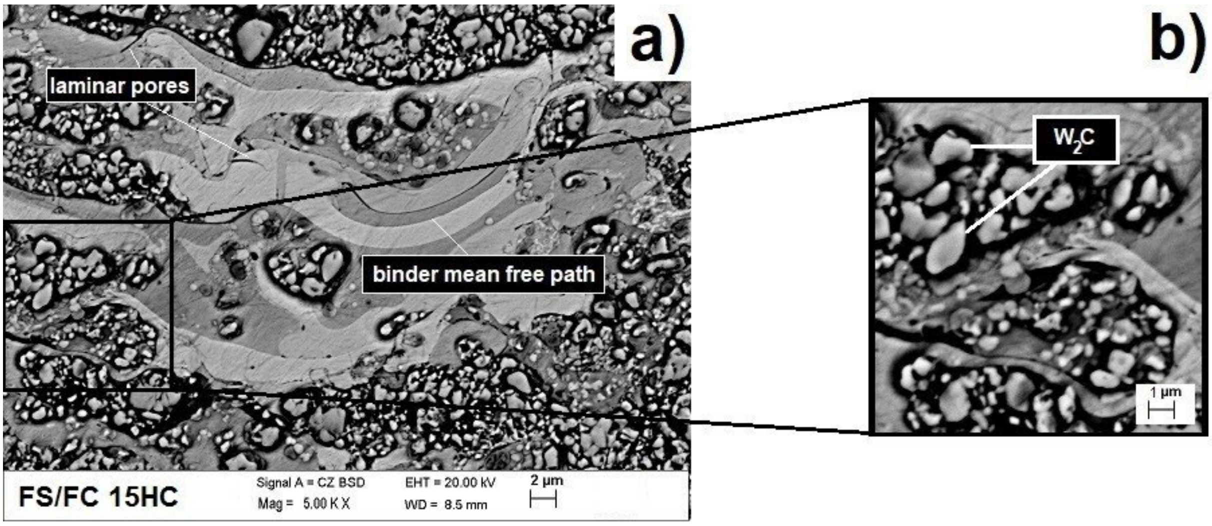

Figure 7. (a) SEM image of the cross section of FS/FC 15 HC material; (b) Detail showing the presence of decarburization in tungsten carbides.

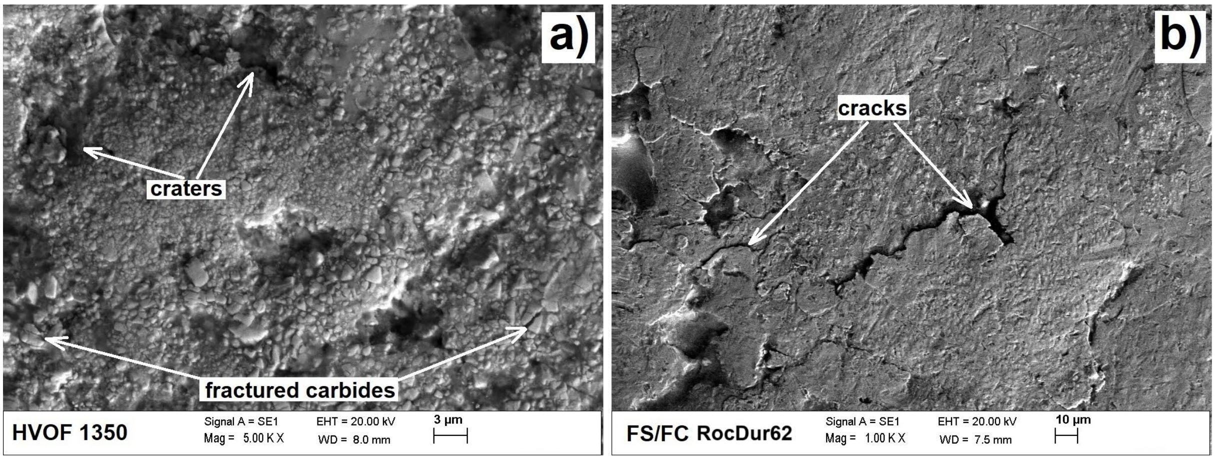

Figure 8. SEM images of the eroded surfaces of materials deposited by HVOF and FS/FC (a) Material HVOF 1350 and (b) Material FS/FC RocDur62.

Regarding the influence of the different variables considered in this study, it is necessary for such analysis to take into account the method of deposition. From the results of the tests, it can be concluded that for all the coatings deposited through the HVOF method, the surface roughness influences the magnitude of the wear evidenced by a valid correlation ($r^2 = 0.7$), however for deposits obtained by FS/FC process this correlation only reaches $r^2 = 0.048$.

A very similar analysis is evidenced by the porosity parameter. In coatings deposited by HVOF, the correlation between Er values and porosity is linear and directly proportional, with a curve fitting of 0.93. In this case, Er increases with the increase in porosity, which shows the significant influence of this factor. However, for the coatings deposited by FS/FC there is a greater dispersion of the data that cause a correlation coefficient of $r^2 = 0.031$, which allows to affirm that the porosity does not considerably influence the erosion rate.

From the analysis of porosity and surface roughness it is deduced that both factors are influential in the erosive wear behavior of the coatings deposited by HVOF, being other factors that take control of this behavior for those deposited by FS/FC, such as the microstructure, the mechanical properties and characteristic defects of the projection process.

According to the results of Er in the critical experimental condition of the erosion tests, it can be affirmed that there is an inversely proportional relationship between Er and Hv, independently of the projection method used in the preparation of the coatings.

In addition to the coatings microhardness, the microhardness of the erosive particles is important to understand the mechanism of the erosive wear, which was confirmed through the indicator that relates to both the microhardness of the deposited material (HvM) and the erosive particles microhardness (HvP) [27]-[29].

When the indicator fulfills the condition $HvM/HvP > 1$ (WC coating deposited by the HVOF method), because the microhardness of the coatings is greater than the erosive particles, abrasive particles can hardly cause the plastic flow in the coating material and the selective nature of the erosion prevails, being minor the damage in the surfaces and therefore less the value of the erosion rate. In this case, the microhardness of the coating material plays a fundamental role in the wear behavior [29].

When the erosive particles microhardness is greater than that of the coating material, then $HvM/HvP < 1$, in this case the crack initiation is inevitable and its propagation factor is what controls the wear rate, which will cause higher values of the erosion rate. Here, the fracture toughness will determine the behavior of the wear, being the microhardness less significant [29]. In a conclusive way it can be affirmed that in the coatings deposited by HVOF and by FS/FC, the microhardness and the fracture toughness play a predominant role in the behavior of the erosion rate.

3.3. Corrosion Test: Polarization Curves

Figure 9 and **Figure 10** show the polarization curves obtained in the electrochemical corrosion tests in the corrosive medium 0.1 M H_2SO_4 with 19 g/L of CL^- for original samples and eroded samples. In all cases, a tendency to passivation of surfaces is observed to a greater or lesser extent.

The coating material FS/FC 15 HC has, for example, a more positive corrosion potential for the original and passive samples at lower current values than the rest of the coatings, as a result of the beneficial effect of the NiCr matrix. The rest of the deposits have a very similar behavior and it is only to point out a slightly lower corrosion potential for the HVOF 1350 material and the tendency to transpassivation of the RocDur62 material that may be related to the high roughness and porosity of the deposit (**Figure 9**).

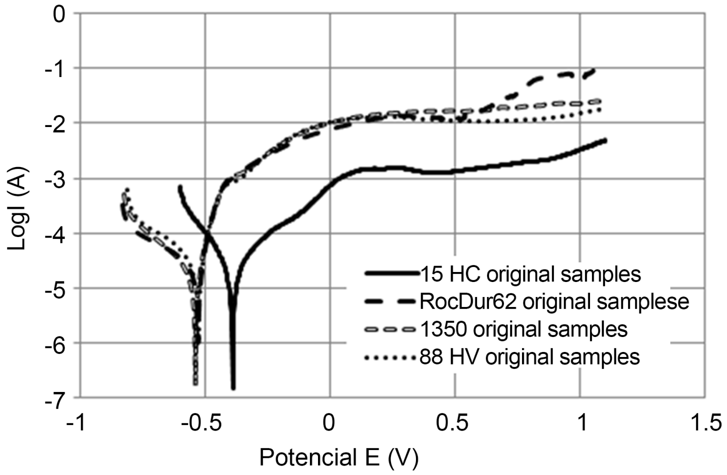

Figure 9. Polarization curves (0.1 M H_2SO_4 with 19 g/L of CL^-) from original samples.

Figure 10 shows the polarization curves of the previously eroded samples. As can be seen, all the samples tested maintained their passivation capacity with very close values of the current to the original samples and less noble potentials. However, the passivation of the eroded samples is more stable, which may be related to the surface roughness of these coatings, which decreases significantly during the erosion tests, as expected [30]-[34].

Figure 11 shows the micrographs of the FS/FC 15 HC coating for both conditions, corroded original samples and those previously eroded and subsequently subjected to corrosion.

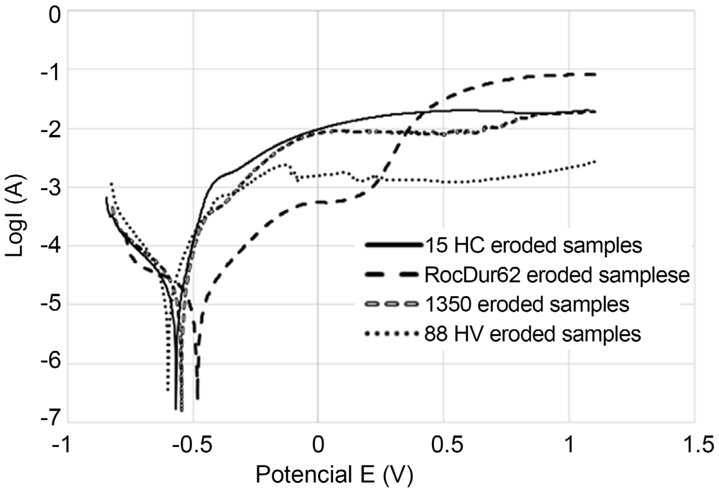

Figure 10. Polarization curves of the corroded samples (0.1 M H_2SO_4 with 19 g/L of CL^-) after the erosion test.

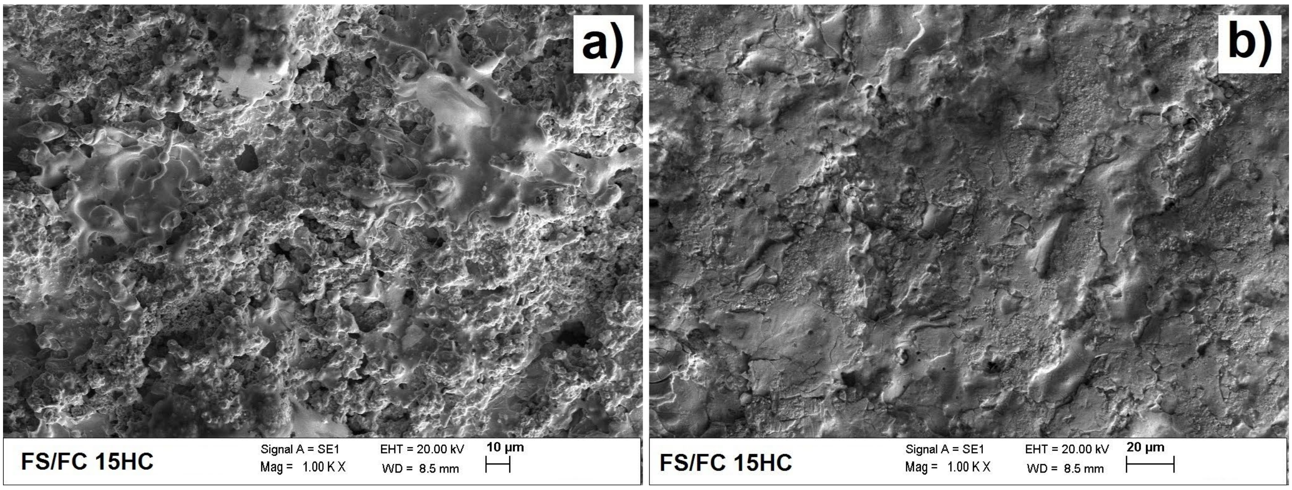

Figure 11. Micrographs SEM 15HC coating (a) corroded original sample, (b) sample previously eroded and corroded.

As can be seen in the previous figure, the corrosive process begins with the dissolution of the binder phase depending on the integrity and thickness of the passivated layer, an observation that has been reported by several authors [17] [35].

The dissolution of the binder matrix in the binder/hard phase interface can be considered as a contribution of the corrosive process to mechanical-corrosive wear. The behavior of this material under conditions of erosive-corrosive wear is also influenced by the defects related to the deposition process (high porosity, ~5%, cavities, cracks) that allow a greater penetration of the electrolyte and damage the coating in greater thickness and favor, as was commented, the erosive process. It is significant that although between the original samples, 15 HC presented the most noble potential values and that passivation occurs at lower current values, however for the eroded samples this coating presents a lower mechanical resistance of the passivation film which can be related according to Shipway [36] to that during the erosion process preferentially removes the binder phase followed by the extrusion of carbides, process that for the alloy is very aggressive in acidic media. In this sense also mean that it has been reported for the literature that the WC/Ni system passes from a system of passivity to a very active corrosion in corrosive erosive media Cl^- [35].

A different behavior presented RocDur62 coating (**Figure 9** and **Figure 12**) with the most noble corrosion potential and with a first transpassivation at a potential of 0.2 V while for the original sample the first break of the passive layer occurs at a potential of 0.5 V, which can be related to settlement and the great decrease in roughness due to the action of abrasive particles (Ra = 6.2 µm by 4.5 µm material 15 HC) and the ability of NiCrBSiFe alloy to generate protective layers.

The coatings deposited by HVOF, however, almost did not show significant differences in their behavior between the original samples and those previously eroded (**Figure 13**).

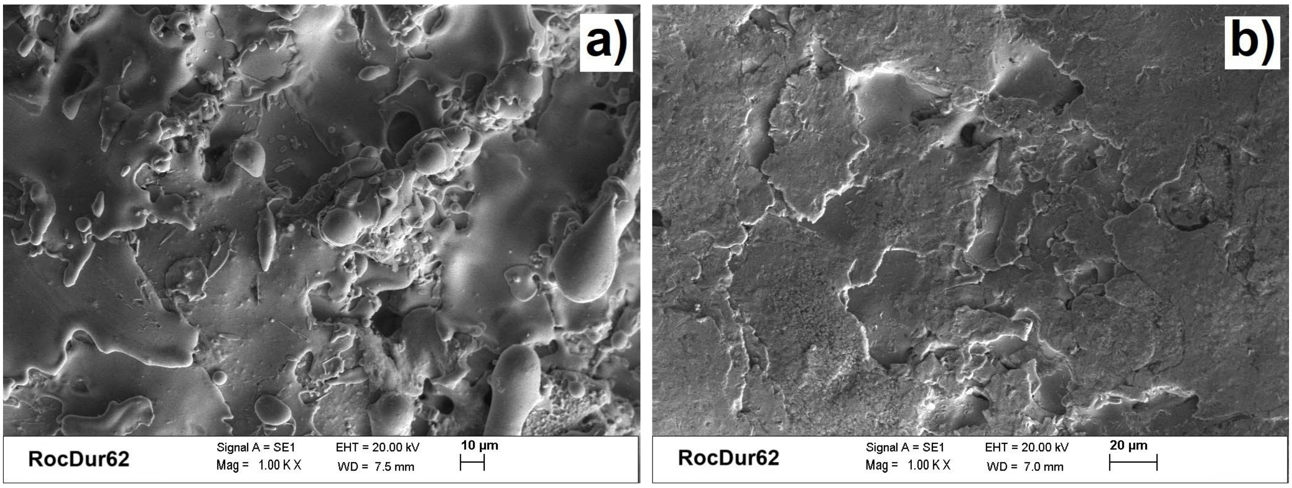

Figure 12. SEM images for coating RocDur62. (a) Original sample corroded; (b) Sample previously eroded and corroded.

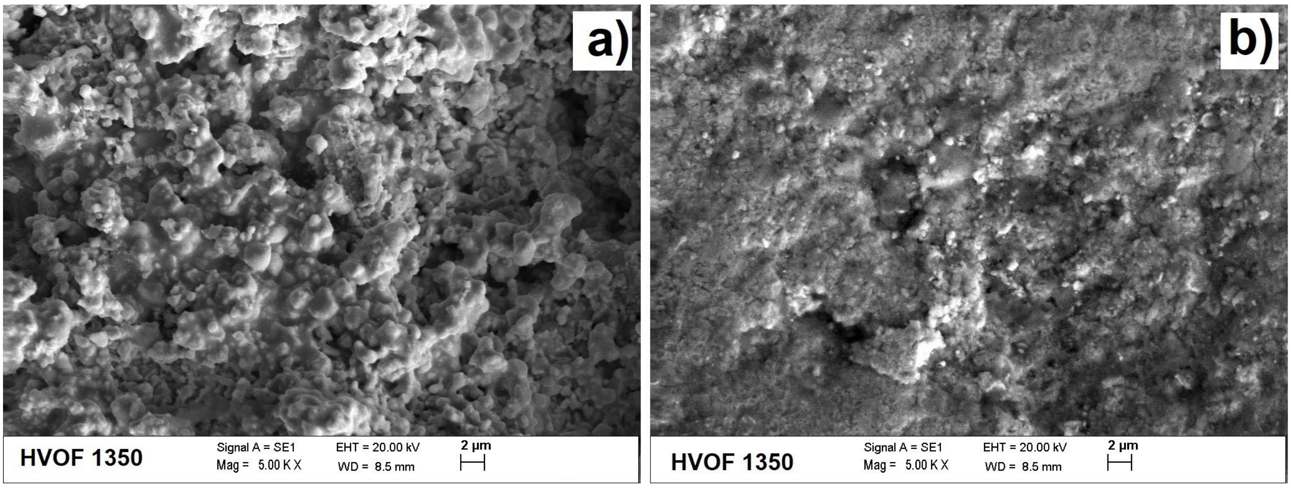

Figure 13. SEM micrographs of the HVOF 1350 coating. (A) Corroded original samples; (b) Eroded and corroded samples.

For this coating (HVOF 1350), the attack under static conditions begins at the interface between the carbides and the matrix in the form of pitting and cavities, which is very important since it establishes the sustainability of the hard phase in the matrix and plays an important role in the mechanical properties (hardness, mechanical strength and toughness) The surface of the previously eroded material reveals the skeleton of the hard phase to the surface and the corrosion intensifies the extrusion process of the carbide grains, but considering under the conditions in which the samples were tested, the material maintains an extensive passivation zone.

HVOF 88 HV coating (**Figure 14**) also showed very little difference in the behavior between the original samples and those previously eroded. The presence of Cr and Si, as alloy elements, play a central role in the development of protective oxides. In summary, in this corrosive environment, it can be concluded that the erosion process of the analyzed samples slightly alters the corrosion process of the samples deposited by the HVOF method.

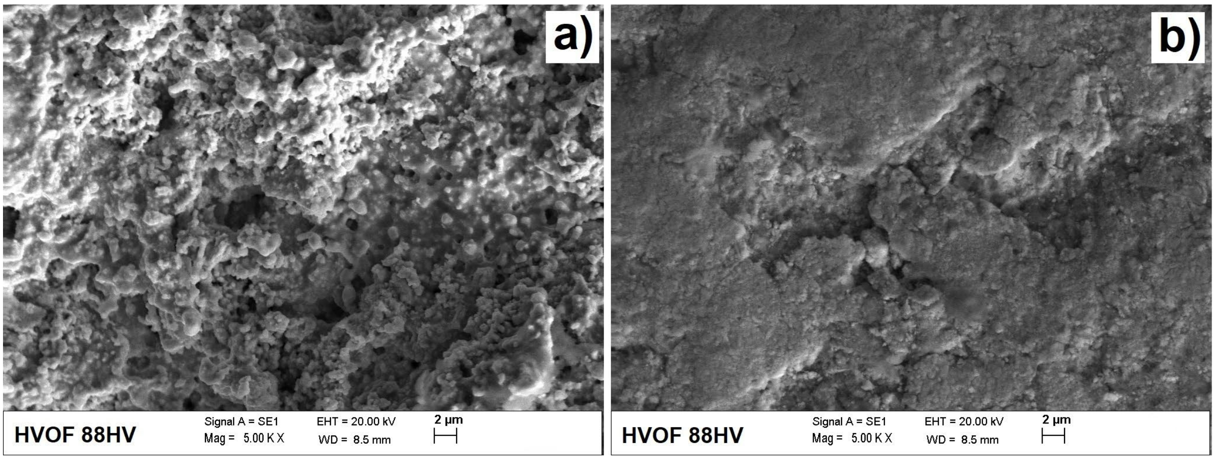

Figure 14. SEM micrographs of the HVOF 88 HV coating (a) Corroded original sample, (b) Previously eroded and corroded.

3.4. Erosion-Corrosion Tests

Figure 15 shows the result of the dynamic erosive-corrosive test, in which the same mixture used in the erosion test was used, adding 5% HCl. Significant differences can be observed regarding the behavior of the materials in relation to the previous tests of erosion and corrosion under static conditions, which show a mechanism in which the erosive component of wear predominates, with an important contribution from the mechanical properties (hardness and toughness), chemical composition, and microstructure.

The synergistic action of erosion-corrosion phenomena is evident. For example, the material 15HC, which has better mechanical properties of FS/FC coatings, presents greater resistance to erosion; however, it shows the lowest erosion-corrosive wear resistance, which can be deduced from the results of the polarization curve of previously eroded samples and the corrosion wear tests.

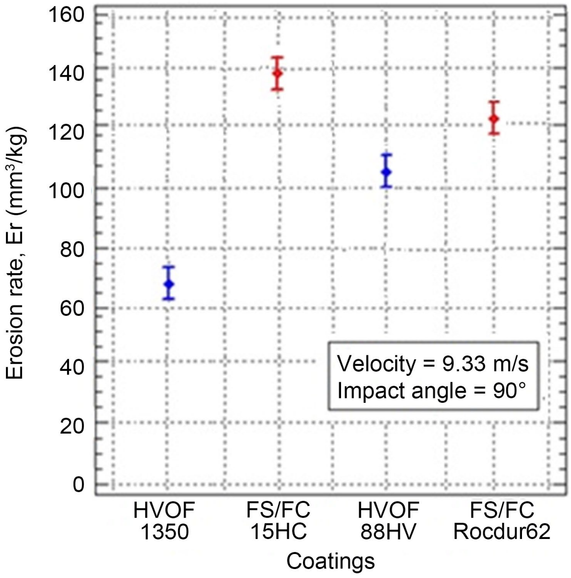

Figure 15. Corrosive wear rate in the dynamic erosive-corrosive test.

Figure 16 shows the SEM micrographs of the different deposits after erosion-corrosion tests. Under the synergistic action, the skeleton of the carbides becomes more visible, which is associated with the faster and greater removal of the binder phase by the combined action of the impact of the erosive particles and the acidic medium. The presence of pitting and cracks, caused by the erosive effect and deepened by the action of the medium, is also more evident, all of which can lead to the extrusion of carbide grains. The previous defects of the material play an important role in the presence of the electrolyte, forming sub superficial deposits that undermine the release of material from the impact of the particles [17] [37] [38].

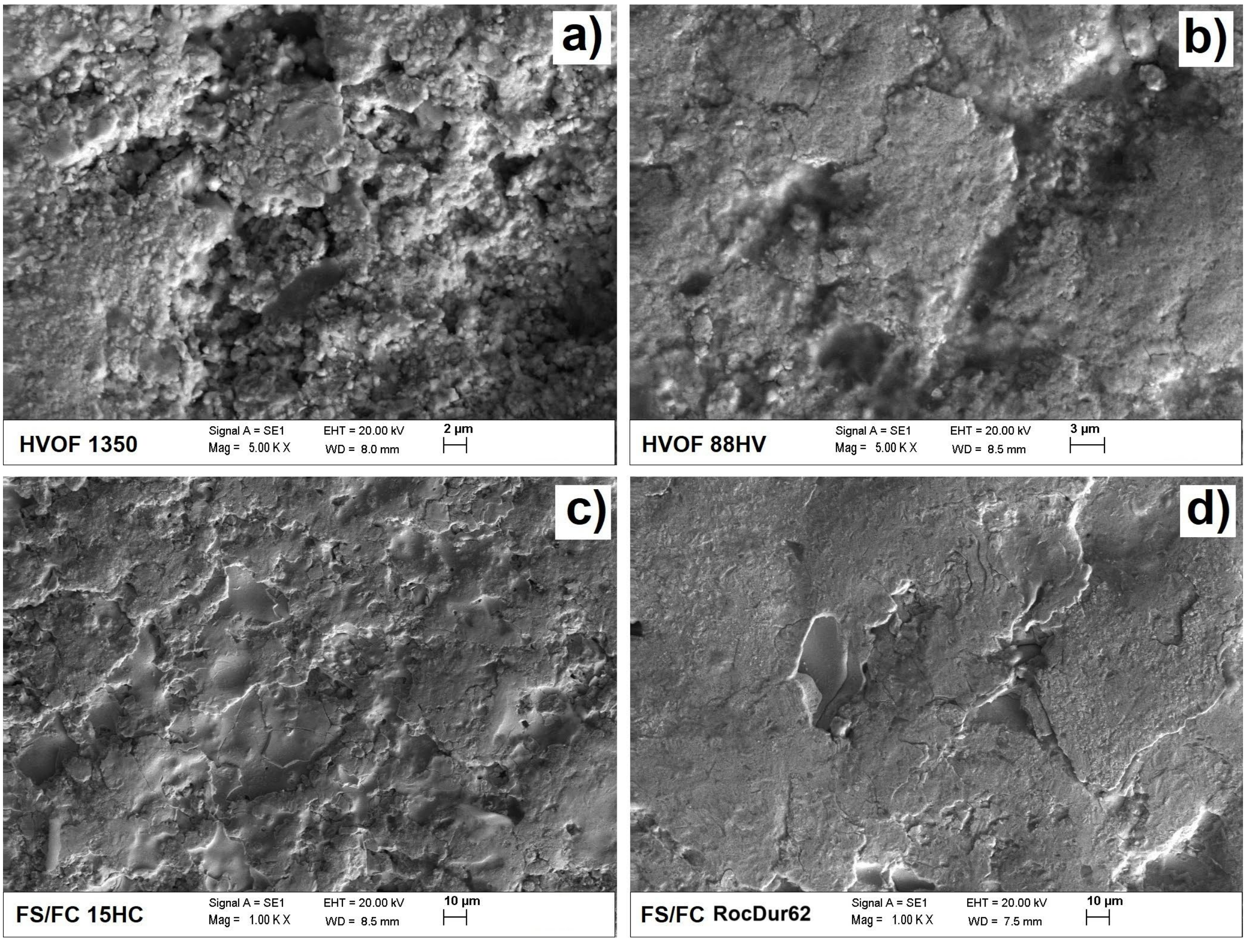

Figure 16. SEM micrographs of the coatings after the dynamic erosive-corrosive test. (a) HVOF 1350; (b) HVOF 88 HV; (c) FS/FC 15 HC; (d) FS/FC RodDur 62.

The magnitude of the damage in these conditions is also associated with the method of deposition beyond what is discussed here in relation to the formation of the W_2C phase. FS/FC method is characterized by the dense projections of binder and hard matrix phases over the substrate that exhibit a low degree of fusion due to the lower flame temperature and which can result in greater mechanical damage to the reinforcing particles which leads to a weaker matrix-filler bond.

For coatings with WC reinforcements, the projection results in a greater proportion of W due to decarburization, leading to an additional effect on the localized corrosion of the material at the interface with the matrix. This affects the behavior of the material FS/FC 15 HC, where it is evident that corrosion increases losses due to the erosion from abrasive particles.

The findings on the erosion-corrosion effect on coatings of materials applied by the studied HVOF and FSFC processes are partially generalizable to other abrasive/corrosive environments, but with important caveats. Findings from 0.1 M H_2SO_4 with 19 g/L of CL may not fully apply to NaCl environments (e.g., seawater), acidic (H_2SO_4) or alkaline (NaOH) media due to differences in corrosion kinetics and passive film stability, as explained by Bjordal *et al.* [32].

The synergistic effect of erosion-corrosion can significantly increase material loss—often exceeding 50% of total wear—due to mutual enhancement between mechanical and chemical degradation. Quantification methods like weight loss partitioning and electrochemical analysis confirm its dominance in many aggressive environments.

In this context, it is interesting to develop materials with enhanced corrosion resistance using a Ni-Cr matrix, increasing the content of other alloys such as B, Si, and Fe. These compositions have a high passivation capacity, and their protective effect is extended appropriately under wear-corrosion conditions. Consequently, under such conditions, hardness, plastic deformation abilities, and transformations of the binder phase also become highly relevant.

4. Conclusions

The study of the behavior of the FS/FC coatings under conditions of erosive-corrosive wear from the microstructural and mechanical characterization allowed to describe the wear mechanism, which in such deposits and by such procedure has not been reported by the literature consulted.

In all the coatings, the presence of a fragile-type wear mechanism was observed, wherein, under the action of repetitive impacts from the erosive particles, surface and subsurface craters and cracks appeared, followed by their propagation, carbide fracture, and lamination processes due to fatigue. Under conditions of low particle velocity (3.61 m/s), there are no significant differences in the wear ratio between the coatings obtained by HVOF and FS/FC, regardless of the impact angle of the erosive particles. Due to the lower application cost (estimated as 9% lower) of the FS/FC process, this result enhances the application of the FS/FC process in similar industrial conditions.

The results of the tests conducted show a wear mechanism in which the erosive component prevails in the wear-corrosion synergy, although the corrosion process plays a decisive role in the magnitude of wear. It is very interesting to develop materials that combine a balance between their mechanical properties (hardness, fracture toughness, plastic deformation abilities) and the transformations of the binder phase.

Acknowledgements

The authors acknowledge the State University of Campinas and OPT Surface Engineering for technical support in the experiments. The authors wish to express their gratitude to the memory of our colleague Dr. Miguel Angel Reyes Mojena.

Conflicts of Interest

The authors declare no conflicts of interest regarding the publication of this paper.

References

[1] Sharma, A.K., Kumar, N. and Das, A.K. (2024) A Review on Wear Failure of Hydraulic Components: Existing Problems and Possible Solutions. *Engineering Research Express*, **6**, Article ID: 012502. https://doi.org/10.1088/2631-8695/ad299f

[2] Qu, S., Li, D., Li, J., Sun, P., Li, X. and Sun, G. (2025) Investigate the Impact Wear Failure Behavior of CoMoCr Engine Valve and Valve Seat Pairs under Harsh Conditions. *Engineering Failure Analysis*, **167**, Article ID: 109052. https://doi.org/10.1016/j.engfailanal.2024.109052

[3] van Dam, J.P.B., Tiringer, U., Abrahami, S.T., Milošev, I., Terryn, H., Kovač, J., *et al.* (2024) Surface Engineering of Aerospace Aluminium Alloys: Understanding Alloying Effects on Chemical Pre-Treatment and Sol-Gel Coating Adhesion. *Surface and Coatings Technology*, **485**, Article ID: 130901. https://doi.org/10.1016/j.surfcoat.2024.130901

[4] Sun, Y. (2023) Surface Engineering & Coating Technologies for Corrosion and Tribocorrosion Resistance. *Materials*, **16**, Article 4863. https://doi.org/10.3390/ma16134863

[5] Ali, O., Ahmed, R., Toma, F., Berger, L., Matthey, B., Faisal, N., *et al.* (2023) Influence of Feedstock and Thermal Spray Process on the Phase Composition of Alumina Coatings and Their Sliding Wear. *Journal of Thermal Spray Technology*, **32**, 2028-2053. https://doi.org/10.1007/s11666-023-01597-z

[6] Memon, H., Rincón Romero, A., Derelizade, K., Venturi, F. and Hussain, T. (2022) A New Hybrid Suspension and Solution Precursor Thermal Spray for Wear-Resistant Silicon Carbide Composite Coatings. *Materials & Design*, **224**, Article ID: 111382. https://doi.org/10.1016/j.matdes.2022.111382

[7] Saint-Gobain Coating Solutions, Thermal Spray Flexicords. https://www.globalspec.com/FeaturedProducts/Detail/SaintGobainCoatingSolutions/113455/Thermal_Spray_Flexicords

[8] Villa, M., Dosta, S., Fernández, J. and Guilemany, J.M. (2012) La proyección fría (CGs): Una alternativa a las tecnologías convencionales de deposición. *Revista de Metalurgia*, **48**, 175-191. https://doi.org/10.3989/revmetalm.1111

[9] Wheeler, D.W. and Wood, R.J.K. (2005) Erosion of Hard Surface Coatings for Use in Offshore Gate Valves. *Wear*, **258**, 526-536. https://doi.org/10.1016/j.wear.2004.03.035

[10] Valentinelli, L., Valente, T., Casadei, F. and Fedrizzi, L. (2004) Mechanical and Tribocorrosion Properties of HVOF Sprayed Wc-Co Coatings. *Corrosion Engineering, Science and Technology*, **39**, 301-307. https://doi.org/10.1179/174327804x13884

[11] Mojena, M.A.R., Roca, A.S., Zamora, R.S., Orozco, M.S., Fals, H.C. and Lima, C.R.C. (2017) Neural Network Analysis for Erosive Wear of Hard Coatings Deposited by

Thermal Spray: Influence of Microstructure and Mechanical Properties. *Wear*, **376**, 557-565. https://doi.org/10.1016/j.wear.2016.12.035

[12] Reyes-Mojena, M.Á., Sánchez-Orozco, M., Carvajal-Fals, H., Sagaro Zamora, R. and Camello-Lima, C.R. (2017) A Comparative Study on Slurry Erosion Behavior of HVOF Sprayed Coatings. *DYNA*, **84**, 239-246. https://doi.org/10.15446/dyna.v84n202.56542

[13] Vinod Kumar, M.S., Suresh, R. and Jegadeeswaran, N. (2022) Study of Solid Particle Erosion of Thermal Spray Coated and Uncoated Cobalt Based Superalloy. *Journal of Mines, Metals and Fuels*, **69**, 31-36. https://doi.org/10.18311/jmmf/2021/30091

[14] Kumar, A., Sharma, A. and Goel, S.K. (2016) Erosion Behaviour of Wc-10Co-4Cr Coating on 23-8-N Nitronic Steel by HVOF Thermal Spraying. *Applied Surface Science*, **370**, 418-426. https://doi.org/10.1016/j.apsusc.2016.02.163

[15] Wayne, S.F. and Sampath, S. (1992) Structure/Property Relationships in Sintered and Thermally Sprayed WC-Co. *Journal of Thermal Spray Technology*, **1**, 307-315. https://doi.org/10.1007/bf02647158

[16] Yao, J., Liu, F., Tan, L., Huang, L. and Liu, Y. (2024) Decarburization Control and Performance Enhancement: Optimizing HVOF Sprayed Submicron WC-12Co Coating with Additives. *International Journal of Refractory Metals and Hard Materials*, **124**, Article ID: 106846. https://doi.org/10.1016/j.ijrmhm.2024.106846

[17] Wood, R.J.K. (2007) Tribo-Corrosion of Coatings: A Review. *Journal of Physics D: Applied Physics*, **40**, 5502-5521. https://doi.org/10.1088/0022-3727/40/18/s10

[18] Toma, D., Brandl, W. and Marginean, G. (2001) Wear and Corrosion Behaviour of Thermally Sprayed Cermet Coatings. *Surface and Coatings Technology*, **138**, 149-158. https://doi.org/10.1016/s0257-8972(00)01141-5

[19] Barber, J., Mellor, B.G. and Wood, R.J.K. (2005) The Development of Sub-Surface Damage during High Energy Solid Particle Erosion of a Thermally Sprayed WC-Co-Cr Coating. *Wear*, **259**, 125-134. https://doi.org/10.1016/j.wear.2005.02.008

[20] Satya, N.W. and Winarto, W. (2020) Microstructure, Hardness, and Surface Cracks Evaluation of HVOF-Sprayed Stellite-1 Coating Applied on Steam Turbine Blade. *Key Engineering Materials*, **833**, 80-84. https://doi.org/10.4028/www.scientific.net/kem.833.80

[21] Grujicic, M., Sellappan, V., Mears, L., Xuan, X., Seyr, N., Erdmann, M., *et al.* (2008) Selection of the Spraying Technologies for Over-Coating of Metal-Stampings with Thermo-Plastics for Use in Direct-Adhesion Polymer Metal Hybrid Load-Bearing Components. *Journal of Materials Processing Technology*, **198**, 300-312. https://doi.org/10.1016/j.jmatprotec.2007.07.011

[22] López Cantera, E. and Mellor, B.G. (1998) Fracture Toughness and Crack Morphologies in Eroded WC-Co-Cr Thermally Sprayed Coatings. *Materials Letters*, **37**, 201-210. https://doi.org/10.1016/s0167-577x(98)00092-5

[23] Jacobs, L., Hyland, M.M. and De Bonte, M. (1998) Comparative Study of WC-Cermet Coatings Sprayed via the HVOF and the HVAF Process. *Journal of Thermal Spray Technology*, **7**, 213-218. https://doi.org/10.1361/105996398770350954

[24] Fu, D., Xiong, H. and Wang, Q. (2016) Microstructure Evolution and Its Effect on the Wear Performance of HVOF-Sprayed Conventional WC-Co Coating. *Journal of Materials Engineering and Performance*, **25**, 4352-4358. https://doi.org/10.1007/s11665-016-2278-y

[25] Babu, P.S., Basu, B. and Sundararajan, G. (2011) The Influence of Erodent Hardness on the Erosion Behavior of Detonation Sprayed WC-12Co Coatings. *Wear*, **270**, 903-913. https://doi.org/10.1016/j.wear.2011.02.019

[26] Vashishtha, N., Khatirkar, R.K. and Sapate, S.G. (2017) Tribological Behaviour of HVOF Sprayed WC-12Co, WC-10Co-4Cr and Cr_3C_2-25NiCr Coatings. *Tribology International*, **105**, 55-68. https://doi.org/10.1016/j.triboint.2016.09.025

[27] Hussainova, I. (2005) Microstructure and Erosive Wear in Ceramic-Based Composites. *Wear*, **258**, 357-365. https://doi.org/10.1016/j.wear.2004.01.024

[28] Hussainova, I., Kubarsepp, J. and Pirso, J. (2001) Mechanical Properties and Features of Erosion of Cermets. *Wear*, **250**, 818-825. https://doi.org/10.1016/s0043-1648(01)00737-2

[29] Xie, Y., Pei, X. and Wei, S. (2016) Investigation of Erosion Resistance Property of WC-Co Coatings. *International Journal of Surface Science and Engineering*, **10**, 365-374. https://doi.org/10.1504/ijsurfse.2016.077536

[30] Lima, M.M., Godoy, C., Modenesi, P.J., Avelar-Batista, J.C., Davison, A. and Matthews, A. (2004) Coating Fracture Toughness Determined by Vickers Indentation: An Important Parameter in Cavitation Erosion Resistance of WC-Co Thermally Sprayed Coatings. *Surface and Coatings Technology*, **177**, 489-496. https://doi.org/10.1016/s0257-8972(03)00917-4

[31] Fedrizzi, L., Valentinelli, L., Rossi, S. and Segna, S. (2007) Tribocorrosion Behaviour of HVOF Cermet Coatings. *Corrosion Science*, **49**, 2781-2799. https://doi.org/10.1016/j.corsci.2007.02.003

[32] Bjordal, M., Bardal, E., Rogne, T. and Eggen, T.G. (1995) Erosion and Corrosion Properties of WC Coatings and Duplex Stainless Steel in Sand-Containing Synthetic Sea Water. *Wear*, **186**, 508-514. https://doi.org/10.1016/0043-1648(95)07148-2

[33] Bjordal, M., Bardal, E., Rogne, T. and Eggen, T.G. (1995) Combined Erosion and Corrosion of Thermal Sprayed WC and CrC Coatings. *Surface and Coatings Technology*, **70**, 215-220. https://doi.org/10.1016/0257-8972(94)02266-s

[34] Çelik, E., Şengil, İ.A. and Avcı, E. (1997) Effects of Some Parameters on Corrosion Behaviour of Plasma-Sprayed Coatings. *Surface and Coatings Technology*, **97**, 355-360. https://doi.org/10.1016/s0257-8972(97)00208-9

[35] Souza, V.A.D. and Neville, A. (2003) Linking Electrochemical Corrosion Behaviour and Corrosion Mechanisms of Thermal Spray Cermet Coatings (Wc-CrNi and WC/CrC-CoCr). *Materials Science and Engineering: A*, **352**, 202-211. https://doi.org/10.1016/s0921-5093(02)00888-2

[36] Shipway, P.H. and Howell, L. (2005) Microscale Abrasion-Corrosion Behaviour of WC-Co Hardmetals and HVOF Sprayed Coatings. *Wear*, **258**, 303-312. https://doi.org/10.1016/j.wear.2004.04.003

[37] Lima, C.R.C., Batista, J.A., Libardi, R., Fals, H.C., Zamora, R.S., Ribeiro, J.R.S., *et al.* (2015) Developing Alternative Coatings for Repair and Restoration of Pumps for Caustic Liquor Transportation in the Aluminum and Nickel Industry. *Surface and Coatings Technology*, **268**, 123-133. https://doi.org/10.1016/j.surfcoat.2014.08.010

[38] Souza, V.A.D. and Neville, A. (2007) Aspects of Microstructure on the Synergy and Overall Material Loss of Thermal Spray Coatings in Erosion-Corrosion Environments. *Wear*, **263**, 339-346. https://doi.org/10.1016/j.wear.2007.01.071